Innovative Infrastructure Solutions (2021) 6:23
https://doi.org/10.1007/s41062-020-00390-z

TECHNICAL PAPER

Influence of compressive load on concrete filled steel tubular column with variable thickness

Dhiraj Ahiwale[1] · Rushikesh Khartode[1] · Akshay Bhapkar[1] · Giridhar Narule[1] · Kamalkishor Sharma[1]

Received: 3 July 2020 / Accepted: 12 October 2020 / Published online: 22 October 2020

Abstract

The concrete-filled tubular (CFT) structure consists of high strength, favourable ductility, fire resistance and huge energy absorption. The cost and time of construction can be reduced as there is no shuttering required for CFT columns. The confinement outcome of CFT column possesses higher stiffness as compared to hollow steel tube columns.

In this article, testing is administered on twelve specimens of natural and artificial sand M25 grade CFT columns with a ratio of diameter to variable tube thickness (D/t of 27.72, 22.18 and 18.48). The twelve CFT columns have been tested under axial compression. The behaviour of CFT columns has been studied in terms of axial load-carrying capacity, deflection and buckling effects and compared the behaviour with numerical results determined using Eurocode 4 and AISC 360-10. The performance of CFT columns increased, as the thickness of tube increased with the effective confinement. The experimental and the numerical results of CFT columns have been validated by using ANSYS 14.5. The axial load-carrying capacity of an artificial sand CFT specimen has been improved significantly. Therefore, the natural sand could be replaced with artificial sand for CFT columns.

Keywords CFT · Load-carrying capacities · Buckling · Eurocode 4 · AISC 360-10 · ANSYS

Introduction and literature review

Concrete and steel are the foremost extensively used and consumed materials within the construction of building structures. The fashionable developments within the construction sector prove further inclination towards the development of RCC multi-story structures everywhere in the planet. The planning of such high-rise structures demands huge components, particularly columns resulting in the introduction of huge axial forces and moments. Due to continuous efforts of researchers, the CFT column is a highly developed system in the building of structures. However, CFT column sections like circular, rectangular, square, octagonal, polygonal and elliptical are widely used in the engineering structures. But there is more local buckling in square or rectangular CFT columns due to less confinement by steel tube and concrete when compared to circular CFT column [1–9].

Many researchers have studied the close behaviour of CFT column and suggested the design guidelines for analysis [4, 6, 7]. The concrete-filled tube columns also are called as composite columns which are extensive important parts in composite structures. A lot of research has been performed on the experimental and numerical investigation with the purpose to review the performance of concrete-filled tube specimens with different grades of steel and variable thicknesses like mild steel, aluminium, high strength steel and many more. A numerical study has been conducted to estimate the buckling failure causing the major failure mode found in concrete-filled tube columns and suggests a design rule to prevent this failure [4–8]. An experimental investigation has been conducted to estimate the load-carrying capacity of CFT columns by using different types of sand like quarry dust, concrete debris, sea sand and demolished concrete blocks [10–13]. Many researchers have observed that the artificial sand improves the strength of concrete [14, 15]. Also, a lot of study has been conducted on the load-carrying capacity of CFT columns with recycled aggregate, and from that study, it is observed that the recycled aggregates improve the strength of CFT columns [16–20]. Till date, extensive study has been performed to review the

✉ Dhiraj Ahiwale
dhiraj.ahiwale@vpkbiet.org

[1] Vidya Pratishthan's Kamalnayan Bajaj Institute of Engineering and Technology, Baramati, Pune 413133, India

performance of concrete-filled tube specimens subjected to concentric and eccentric loadings [21–24]. A few researchers have developed FE model and simulated the performance of CFT columns by using finite element software [18, 25]. A lot of efforts have been made by the various researchers in the development of technologies in steel and composite structures. The castellated and cellular beams are the examples of such technologies. The researchers have thoroughly investigated the behaviour of such beams in terms of failure modes, optimization of shape and size of openings [26–31].

Even though there is a broad study on the performance of CFT columns, very few studies have been performed on artificial sand CFST column. Presently, the design procedures for the CFT columns are given in American code (AISC 360-10) [32] and Eurocode (EC-4) [33]. Generally, the number of researchers has studied the natural sand CFT columns. Hence, there is need to study artificial sand CFT columns. Also, results of natural sand and artificial sand CFT column have been validated in ANSYS [38]. Furthermore, the construction of CFT column in India is advanced technology. There is no codal provision of the design rules for CFT columns in Indian code [34]. Therefore, the study has been performed to examine the performance of artificial sand CFT columns constructed with locally available sand collected from vertical shaft impact (VSI) stone crusher. A series of specimens having varying D/t ratios were tested under concentric loading. The primary aim of this study is to test the CFT specimen for variable tube thickness under concentric loading. The secondary aim is to examine the effect of artificial sand concrete in compressive strength and the behaviour of tested columns and thirdly to study the existing design codes (EC-4 and AISC 360-10) for the natural and artificial sand CFT columns.

The conclusion of this study will be benefited for the construction and design of composite column structures. The compressive strength and behaviour of artificial sand CFT specimens are higher than the corresponding natural sand CFT specimens.

Experimental set-up and investigation

The investigation was administered on circular hollow steel column specimens filled with natural and artificial sand concrete of grade M25 having a height of the column of 600 mm with variable wall thickness of 3.2 mm, 4.0 mm and 4.8 mm as shown in Fig. 1 having the modulus of rigidity 76,900 MPa, density 7850 kg/mm^3 and Poisson's ratio 0.3. The Young's modulus of hollow steel tube is 2×10^5 N/mm^2. The ratio of area of steel to concrete is defined as sectional area ratio (α = As /Ac). The steel ratios considered in this study are 0.15, 0.21 and 0.26. The hollow circular tube diameter (D) of 88.70 mm and three variable walls' thickness of 3.2 mm, 4.0 mm and 4.8 mm are chosen as per IS: 1239:2004, clauses 8.1 and 10.1.1.1 [35].

The properties of sand as obtained are presented in Table 1. The artificial sand artificially produced in vertical shaft impact (VSI) crusher was collected from VSI crusher at Vasunde, Pune, Maharashtra, India. A uniformly natural sand and artificial sand (zone- II) as shown in Fig. 2 are used. The ingredient material utilized in this study was collected from local sources. Ordinary Portland Cement of 53 grades was used. Potable water was used during the preparation of concrete mix. Six cubes of grade M25 [37] having the size of 150 mm × 150 mm × 150 mm concrete has been casted, and therefore, the cubes were tested to gauge the strength of concrete. After 28-day curing of specimens, the average compressive strength (f_{cu}) of natural sand and artificial sand concrete was found to be 32.2 MPa and 33.8 Mpa, respectively.

In order to determine the material properties of steel, three coupon specimens of thickness of 3.2 mm, 4.0 mm and 4.8 mm were cut from the steel tube and prepared according to ASTM E8 [36]. The coupon test is shown in Fig. 3. All three specimens were tested for axial tensile test, and obtained results of tensile coupons test for steel tubes are given in Table 2.

The parameters were investigated on a complete twelve specimens of CFT columns under axial compression. The six specimens consists of natural sand (NS) concrete of variable wall thickness 3.2 mm (C3-RS1 and C3-RS2), 4.0 mm (C4-RS1 and C4-RS2) and 4.8 mm (C5-RS1 and C5-RS2), and the remaining six specimens are of artificial sand (AS) concrete of variable wall thickness 3.2 mm (C3-MS1 and C3-MS2), 4.0 mm (C4-MS1 and C4-MS2) and 4.8 mm (C5-MS1 and C5-MS2). The design mix of M25 grade concrete is given in Table 3 [37]. The specimens were cured for twenty-eight days in curing tank for proper bonding. Figure 4 shows the natural and artificial sand CFT specimens.

The capacity of 1000 kN Universal Testing Machine (UTM) was utilized, and all the CFT columns were tested under axial compressive force. The strain gauge was connected on the outside surface at mid height of the specimen to measure the longitudinal deflection, and the lateral deflection was measured by using dial gauge attached to universal testing machine. Both the ends of specimens were hinged, and then after that the application of axial compressive loading was started. The most important intention of this study is to find out the result of natural sand and artificial sand concrete in CFT column with variable tube thickness. The diagrammatic and laboratory test set-up for testing of CFT specimens is as shown in Figs. 5 and 6, respectively. The 5 kN initial load was given to hold the specimen vertically straight. The deflections were recorded at each load

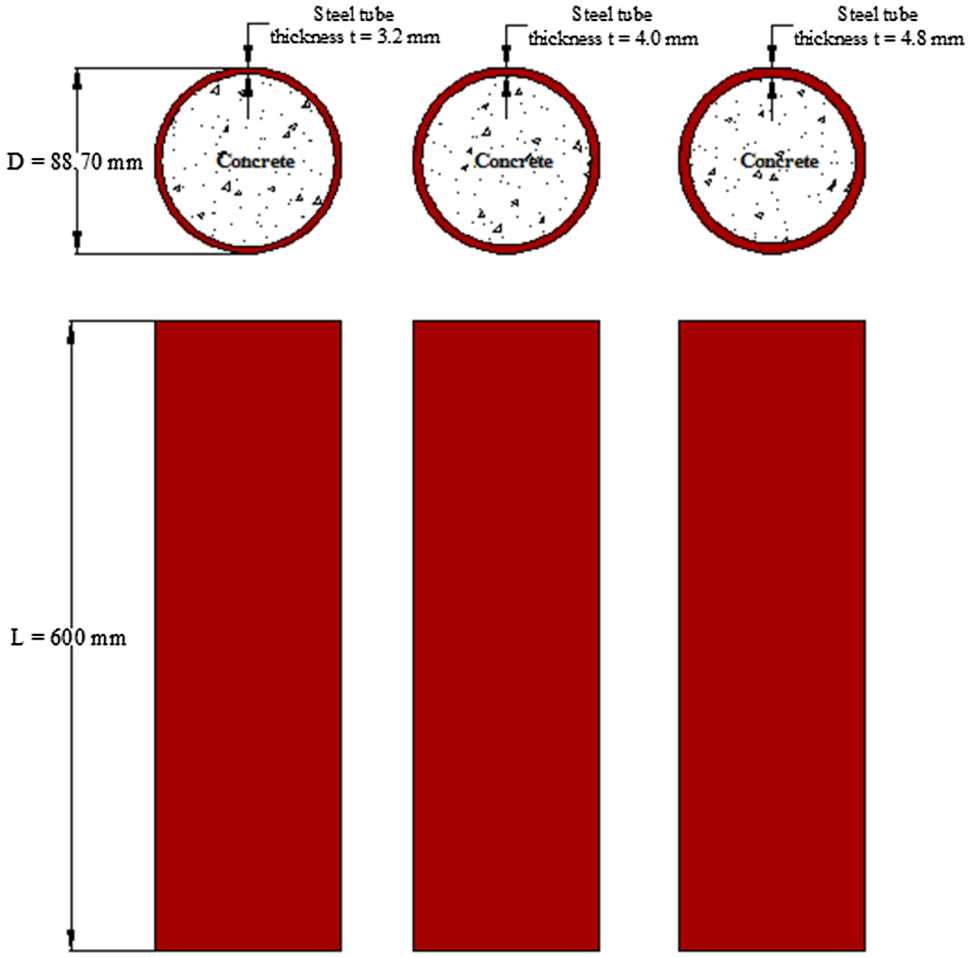

Fig. 1 Plan and side view of specimens with dimensions

Table 1 Properties of concrete materials

Cement		Aggregate			
Physical property	Value	Property	Natural sand	Artificial sand	Coarse aggregate
Fineness	6.02	Specific gravity	2.75	2.94	2.88
Specific surface, m^2/kg	256	Fineness modulus	2.14	4.54	6.10
Normal consistency (%)	33	Water absorption	0.35	0.60	0.72
Initial setting time (min.)	38	–	–	–	–
Final setting time (min.)	227	–	–	–	–
Compressive strength after 28 days (Mpa)	59	–	–	–	–
Specific gravity	3.12	–	–	–	–

increment. The load was applied up to the failure of all CFT specimens. The axial load and deflection were measured during the testing of specimens. The CFT column sections were analysed from the behaviour of load–deflection curves.

Numerical investigation

The maximum load-carrying capacities of natural and artificial sand M25 grade CFT columns are calculated for different D/t ratios by using Eurocode 4 [33] and AISC 360-10 code [32].

Fig. 2 Details of sand

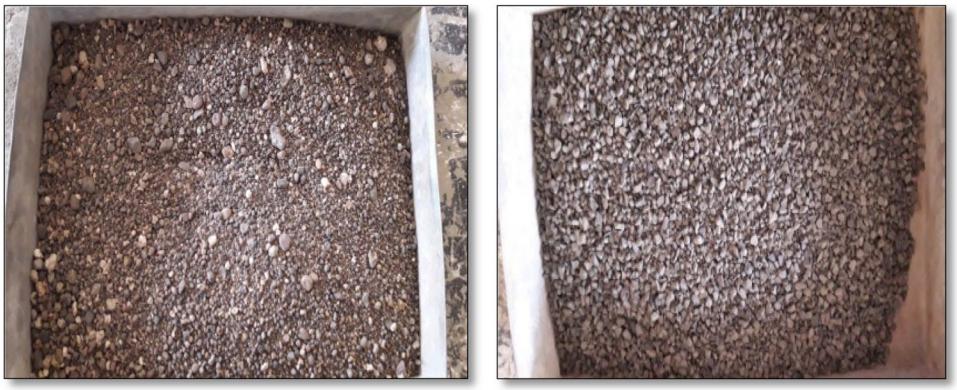

(a) Natural sand **(b)** Artificialsand

Fig. 3 Steel tube coupon test

Table 2 Steel tube coupon test results

Steel tube thickness (mm)	Yield stress (MPa)	Ultimate stress (MPa)	Young's modulus (MPa)	Poisons ratio
3.2	294	476	2×10^5	0.3
4.0	278	443		
4.8	263	410		

Eurocode-4

The maximum load-carrying capacities of CFT columns is calculated by using two coefficients η*1* and η*2* as specified below.

$$P_{\mathrm{p}} = A_{\mathrm{a}}\eta_2 P_{\mathrm{y}} + A_{\mathrm{c}}p_{\mathrm{ck}}[1 + \eta_1] + \mathrm{As}\, p_{\mathrm{sk}}$$

where t is the circular tubular section thickness. $\eta 1$and $\eta 2$ are the two coefficients given by

$$\eta_1 = \eta_{10}\left[1 + \frac{10e}{d}\right] \qquad \eta_2 = \eta_2 + \left(1 - \eta_{20}\right)\frac{10e}{d}$$

The F_{ck} value was taken as:

$$F_{\mathrm{ck}} = 0.83F_{\mathrm{cu}}$$

As an alternative of $F_{\mathrm{ck}} = 0.67F_{\mathrm{cu}}$

where F_{cu} = Concrete cube strength after 28 days.

AISC 360-10 code

The limit state of flexural buckling design is used to determine the maximum load-carrying capacities (ϕPn) and

Table 3 Design mix for normal grade concrete [37]

Mix design	Cement (OPC) (kg/m^3)	Coarse aggregate (kg/m^3)	Natural sand (kg/m^3)	Artificial sand (kg/m^3)	Water kg/m^3)	Avg. f_{cu} (MPa)	Modulus of elasticity in MPa (Ec)
M25	438	1079	880	–	197.1	32.2	28,720
M25	438	1079	–	880	197.1	33.8	29,250

Fig. 4 Details of CFT specimens

(a) Natural sand CFT specimens **(b)** Artificial sand CFT specimens

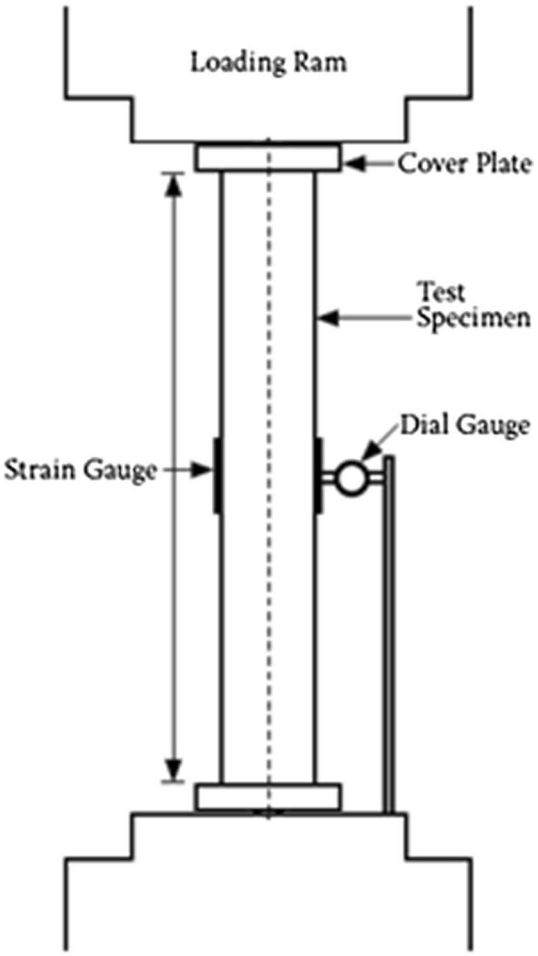

Fig. 5 Diagrammatic test setup

allowable load-carrying capacities (Pn/Ω) for CFT columns as given below:

$$\Phi = 0.75(\text{LRFD}); \quad \Omega = 2.00\,(\text{ASD})$$

(a) When $Pe \geq 0.44P_o$

$$P_n = P_o\left[0.658^{\left(\frac{P_o}{P_e}\right)}0.658^{\left(\frac{P_o}{P_e}\right)}\right]$$

(b) When $Pe < 0.44P_o$;

$$P_n = 0.877P_e$$

$$P_o = A_sF_y + A_{sr}F_{yr} + \text{C2 Acf'c}$$

$C_2 = 0.95$ for circular and 0.85 for rectangular section.

$$P_e = \pi^2(\text{EI}_{\text{eff}})/(\text{KL})^2$$

$$\text{EI}_{\text{eff}} = E_sI_s + C_3E_cI_c$$

$$C_3 = 0.6 + 2\left(\frac{A_s}{A_c + A_s}\right) \leq 0.9$$

where L_{eff} is the effective length of CFT column. The parameters A_s, F_y, E_s and I_s are the area, yield stress, young's modulus and moment of inertia of the steel section respectively and A_c, F_c, E_c and I_c are the area, specified compressive strength, young's modulus and moment of inertia for the concrete respectively.

Analytical investigation

Finite element modelling is usually performed to understand the response of structure for the different type of loading conditions. The modelling precision for specimen is very important; therefore, three-dimensional concrete-filled tube column specimens are formed by providing its height, outer

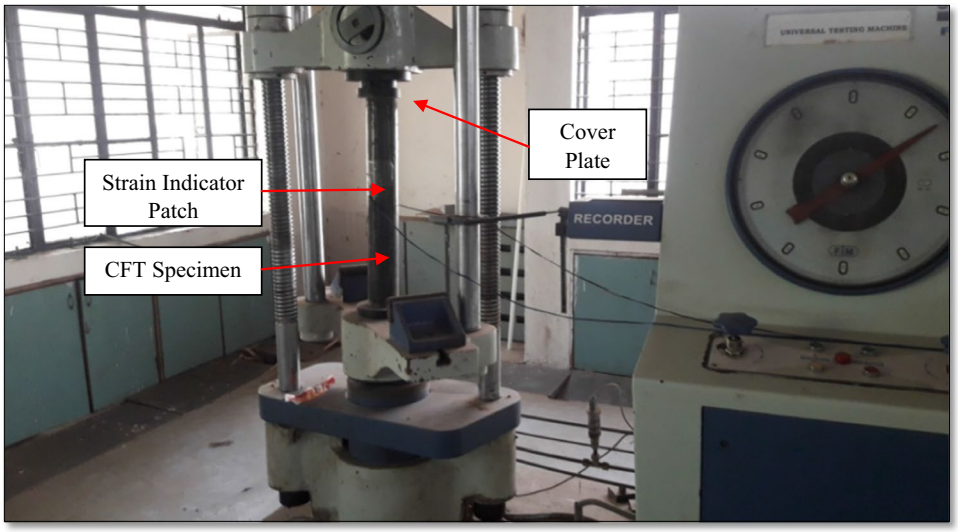

Fig. 6 Laboratory experiment setup

diameter and wall thickness in SolidWorks software and then exported in ANSYS [38] as shown in Fig. 7. To achieve the consistent stress distribution, the concrete tube is modelled as brick elements with three degrees of freedom. The steel tube is modelled as 3D shell element with four-node quadrilateral shell and all node having three translational and three rotational degrees of freedom. In order to calculate the correct results from the finite element model, the three-dimensional hexagonal meshing was discretized in same mesh size to every element in the model to make sure that both the materials share the same node. The compatibility condition for every linking element has been ensured. The property of material given in Table 4 such as Young's modulus, Poisson's ratio, compressive strength, yield stress, ultimate stress and density is assigned to model. The different types of models were developed for different tube thicknesses. The deflection of different model is observed after the experimental load applied to those models. Figure 7 shows the created models of CFT column specimens using ANSYS 14.5 [38]. The compressive force was applied uniformly spread above the top face of column nodes. The force was given in Z-direction and was consent to move in Z-direction but not allowed move in X- and Y-direction. The static structural analysis was performed, and the deflection was checked for variable thickness of natural and artificial sand concrete specimens for compressive force.

Result and discussion

CFT specimen's failure modes

The circular CFT specimens have taken maximum axial compressive load, and it is observed that many specimens have clear view of local buckling over the mid-height. As the function of load increased, the steel has been shows very good ductile deformation and even after severe buckling behaviour, no rupture was observed in the tested CFT specimens. Due to the confinement of CFT specimens, no inward buckling was observed as the internal support provided by core concrete. The most of the specimens were buckled outward, and bulging is also observed in some of the specimen. The buckling behaviour of artificial sand CFT specimens shows better result as compared to natural sand CFT specimens. The tested CFT specimen failure patterns are as shown in Fig. 8.

The deformed shape of the studied artificial and natural sand CFT specimens at failure is as shown in Fig. 9. The artificial and natural sand CFT specimen fails with global lateral buckling because the column is vulnerable to global buckling and due to the restraint from the in filled concrete. The significant local buckling is also observed in the compressive zone above the mid-height of the artificial and natural sand CFT specimen even as slight local buckling is observed at mid-height of the CFT specimen as shown in Fig. 9.

Load–deflection of CFT specimens

The experimental results obtained from natural sand and artificial sand M25 grade CFT column specimens are compared. Also, the experimental outcomes are compared with the analytical outcomes. As per the graphical representations of axial load–deflection performance, the participation of CFT specimens for strain is activated with adopting the use of artificial sand concrete as well as an incremental thickness of wall tube. With also natural or artificial sand concrete infill, the experimentally tested CFT specimens indicate ductile behaviour with no rapid fall of the force. It is obvious that the load–deflection curves exhibited elastic pattern

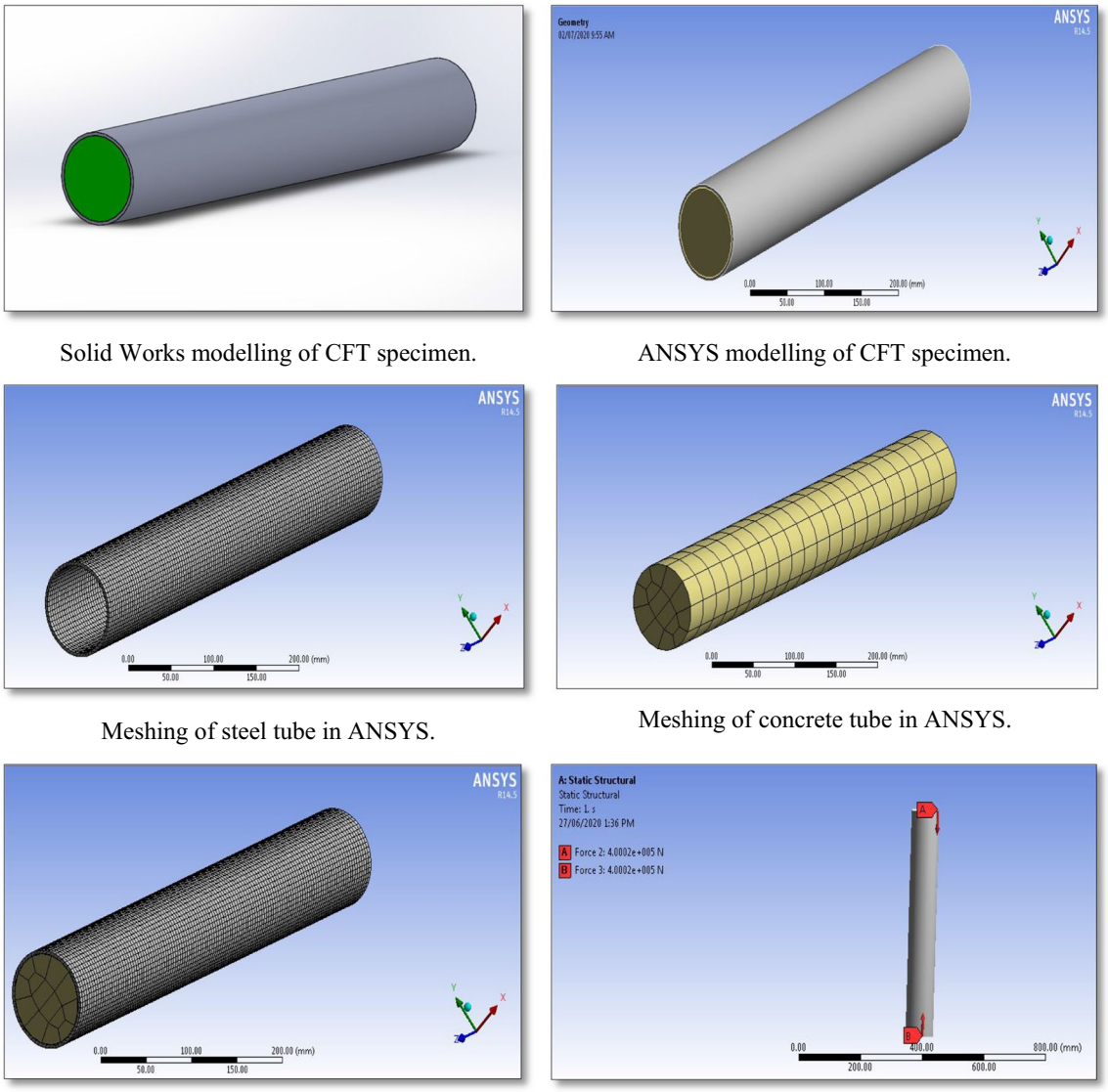

Fig. 7 Modelling and loading of CFT specimen

during the primary loading phase. Then, the steel tube buckled, and therefore, the elastic–plastic phase was reached. The load–deflection curve, peak deflection and peak load for the various types of CFT specimens are given below.

From Figs. 10, 11 and 12, it is observed that the experimental compressive strength of C3-RS, C4-RS and C5-RS is 400 kN, 485 kN and 540 kN, respectively, and the corresponding deflections are 6.4 mm, 4.6 mm and 3.4 mm. Furthermore, from Figs. 13, 14 and 15, the analytical deflection observed for C3-RS, C4-RS and C5-RS is 6.3 mm, 4.5 mm and 3.3 mm, respectively, and the corresponding compressive load is 400 kN, 485 kN and 540 kN.

Similarly, from Figs. 16, 17 and 18, it is observed that the experimental compressive strength of C3-MS, C4-MS and C5-MS is 423 kN, 493 kN and 560 kN, respectively, and the corresponding deflections are 5.9 mm, 4.2 mm and 2.9 mm. Furthermore, from Figs. 19, 20 and 21, the analytical deflection observed for C3-MS, C4-MS and C5-MS is 5.7 mm,

Table 4 Material properties (Elastic)

Material	Properties	Value
Natural sand concrete	Grade of concrete	M25
	Young's modulus (MPa)	28,720
	Poisons ratio	0.2
	Compressive strength (MPa)	32.2
Artificial sand concrete	Grade of concrete	M25
	Young's modulus (MPa)	29,250
	Poisons ratio	0.2
	Compressive strength (MPa)	33.8
Structural steel (3.2 mm thick steel tube)	Young's modulus (MPa)	2×10^5
	Poisons ratio	0.3
	Yield stress (MPa)	294
	Ultimate stress (MPa	476

Fig. 8 Experimental failure modes under compression

3.98 mm and 2.7 mm, respectively, and the corresponding compressive load is 423 kN, 493 kN and 560 kN. Also, it is observed that the artificial sand CFT specimens give the maximum result as compared to natural sand CFT specimens. The artificial sand CFT specimens take an additional compressive force, and its deformation at that compressive force was minimum as compared to natural sand CFT specimens. The analytical and experimental results are 99% similar within the compressive loading investigation.

Comparison of results with design codes

The maximum load-carrying capacities of the tested columns were predicted by using the design philosophies as per the EC4 [33] and AISC 360-10 [32] code. The ultimate load-carrying capacities of D/t ratios 27.72, 22.18 and 18.48 are calculated by using EC-4 [33] and AISC 360-10 [32]. The designed values are consequently compared with the collapse loads gained from the experimental results shown in Table 5 and Fig. 22.

Eurocode 4

Eurocode 4 [33] provides an excellent prediction of the steel tube 4.8-mm-thick specimens (smaller D/t ratio 18.48) when compared to steel tube 3.2-mm and 4.0-mm-thick specimens. For the natural sand CFT columns with 3.2 mm, 4.0 mm and 4.8 mm tube thickness, the major variation among experimental and Eurocode 4 [33] is 22%, 21% and 20%, correspondingly. Meanwhile, for the artificial sand CFT columns with 3.2 mm, 4.0 mm and 4.8 mm tube thickness, the major variation between experimental and Eurocode 4 is 24%, 22% and 22%, respectively. The average Nue/N_{EC4} of the natural sand and the artificial sand CFT columns with 3.2 mm, 4.0 mm and 4.8 mm tube thickness is 1.26 and 1.32, 1.28 and 1.28, 1.25 and 1.29, respectively.

AISC 360-10 code

The load-carrying capacity of experimental results compared with AISC 360-10 [32], and from that study, the results of AISC 360-10 [32] have been found safe for the steel tube thickness of 3.2-mm, 4.0-mm and 4.8-mm specimens. For the natural sand CFT columns with 3.2 mm, 4.0 mm and 4.8 mm tube thickness, the major variation among experimental and Eurocode 4 is 29%, 28% and 26%, correspondingly. Meanwhile, for the artificial sand CFT columns with 3.2 mm, 4.0 mm and 4.8 mm tube thickness, the major variation between experimental and Eurocode 4 is 30%, 29% and 27%, respectively. The average Nue/N_{EC4} of the natural sand and the artificial sand CFT columns with 3.2 mm, 4.0 mm and 4.8 mm tube thickness is 1.41 and 1.44, 1.40 and 1.41, 1.36 and 1.38, correspondingly.

Conclusions

The subsequent conclusions are drawn from the experimental, numerical and analytical investigations carried out on variable tube thickness M25 grade CFT specimens under compressive loading:

From the load–deflection curves for the artificial sand and the natural sand CFT specimens with similar steel tube thickness, it is observed that there is a variation in the load-carrying capacity. However, the thinner steel tube columns have higher bonding capacity compared to thicker steel tube columns.

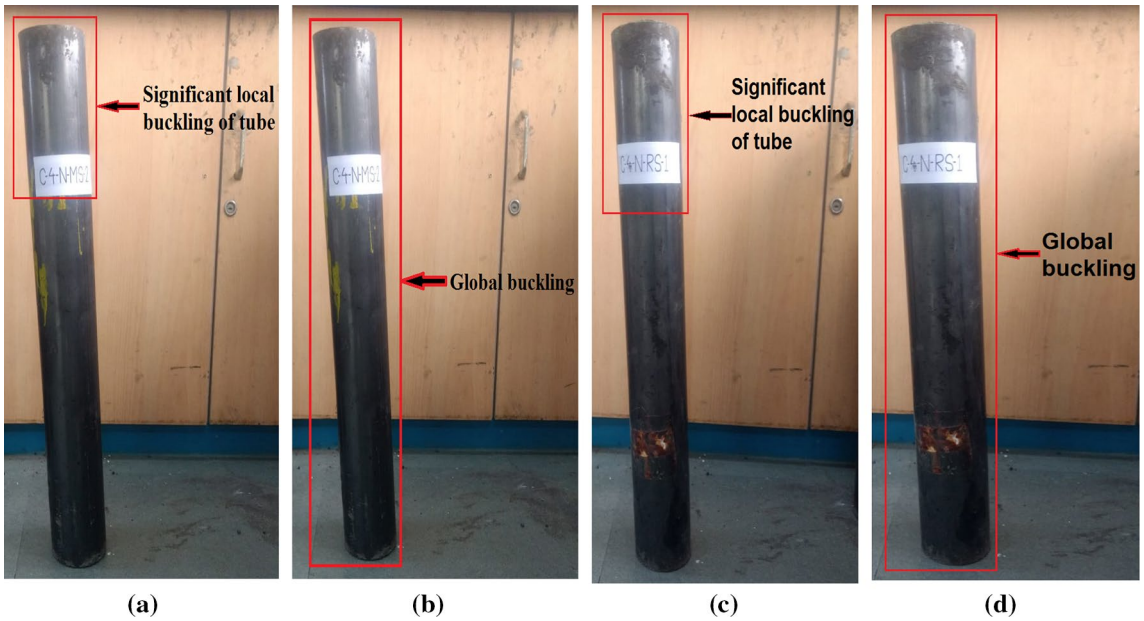

Fig. 9 Typical failure mode of CFT columns: **a** significant local buckling of artificial sand specimen, **b** global buckling of artificial sand specimen, **c** significant local buckling of natural sand specimen, **d** global buckling of natural sand specimen

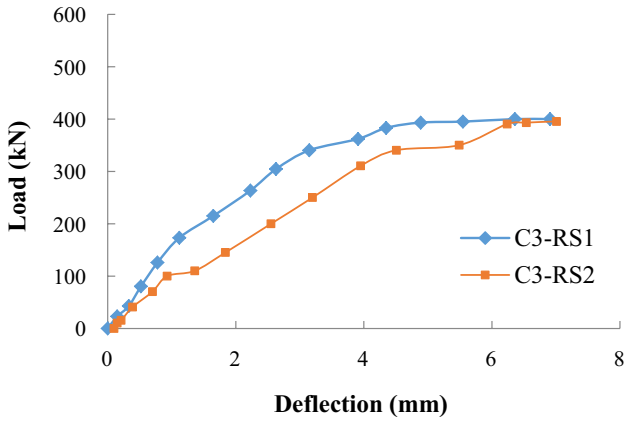

Fig. 10 Load- deflection curve for 3.2 mm thick tube natural sand CFT specimens

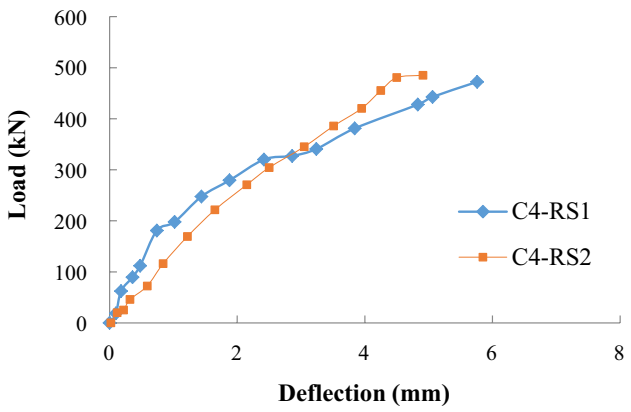

Fig. 11 Load- deflection curve for 4.0 mm thick tube natural sand CFT specimens

The load-carrying capacity of artificial sand CFT specimens is higher than the natural sand CFT specimens with steel tube thickness 3.2 mm, 4.0 mm and 4.8 mm. The load-carrying capacity of artificial sand CFT specimens is increased due to the confinement of the steel tube and concrete. Therefore, to achieve a better economy, the natural sand could be replaced with artificial sand for CFT columns. Furthermore, the thinner steel tube columns have very less load-carrying capacity compared to thicker steel tube columns as bonding effect is not observed to a large extent because of a significant amount of local buckling of the thinner steel tube columns.

The Eurocode 4 [33] and AISC 360-10 [32] codes underestimate the load-carrying capacity for the artificial sand and the natural sand CFT columns. The thinner steel

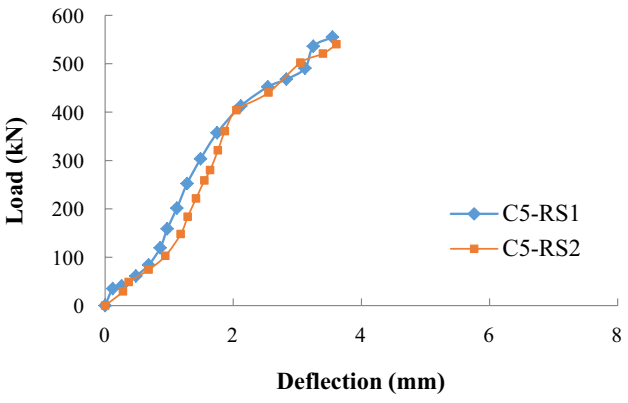

Fig. 12 Load- deflection curve for 4.8 mm thick tube natural sand CFT specimens

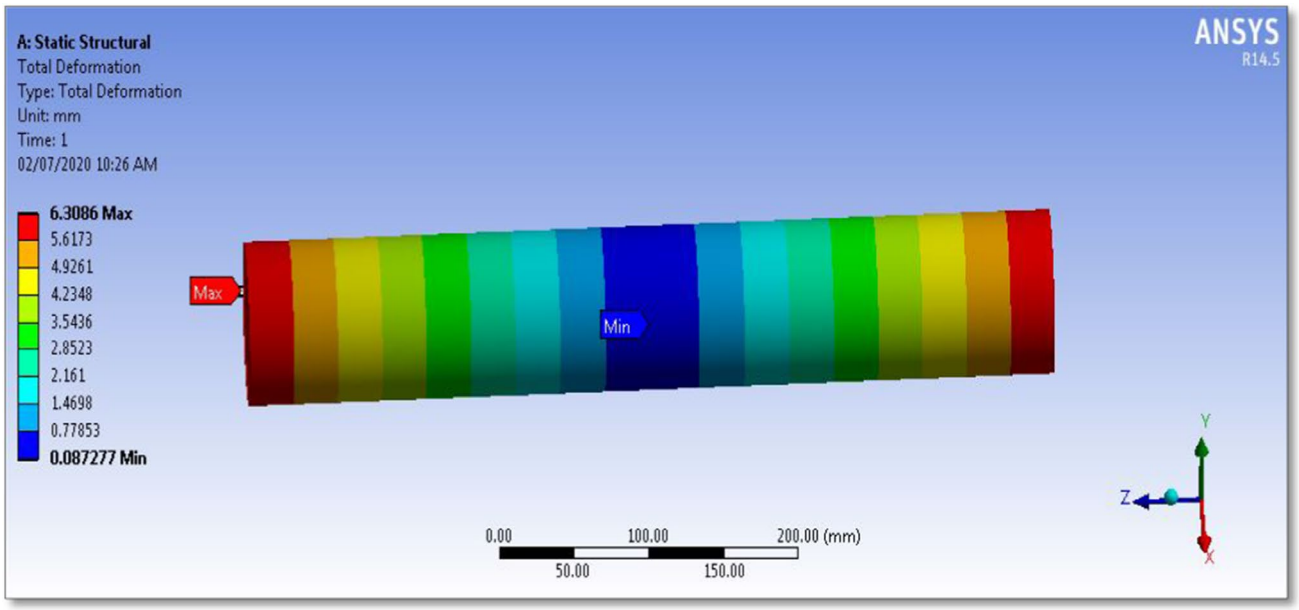

Fig. 13 Deflection under compressive force of 3.2 mm thick tube natural sand CFT specimen

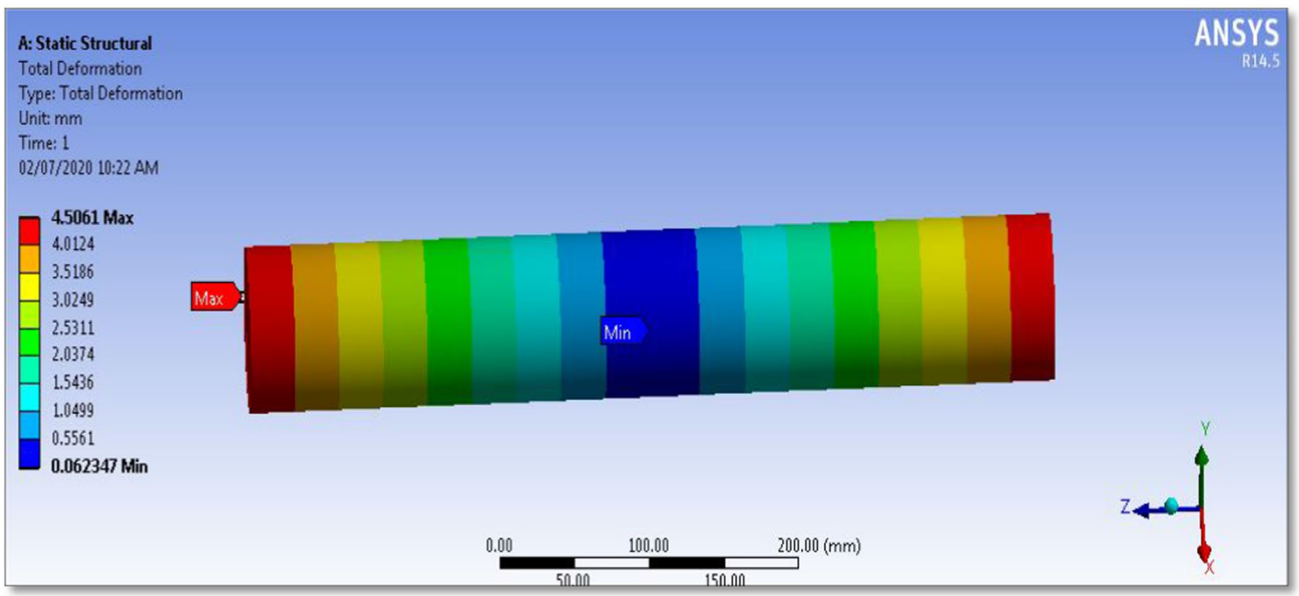

Fig. 14 Deflection under compressive force of 4.0 mm thick tube natural sand CFT specimen

tube columns (D/t is 27.72) show lesser load-carrying capacity because of the steel tube local buckling due to the smaller confinement, and the thicker steel tube columns (D/t is 18.48) show more load-carrying capacity because of the effective confinement by the steel tube to the concrete core. The major variation between experimental results and design codes is 24% and 30% for the Eurocode 4 [33] and AISC 360-10 [32] correspondingly.

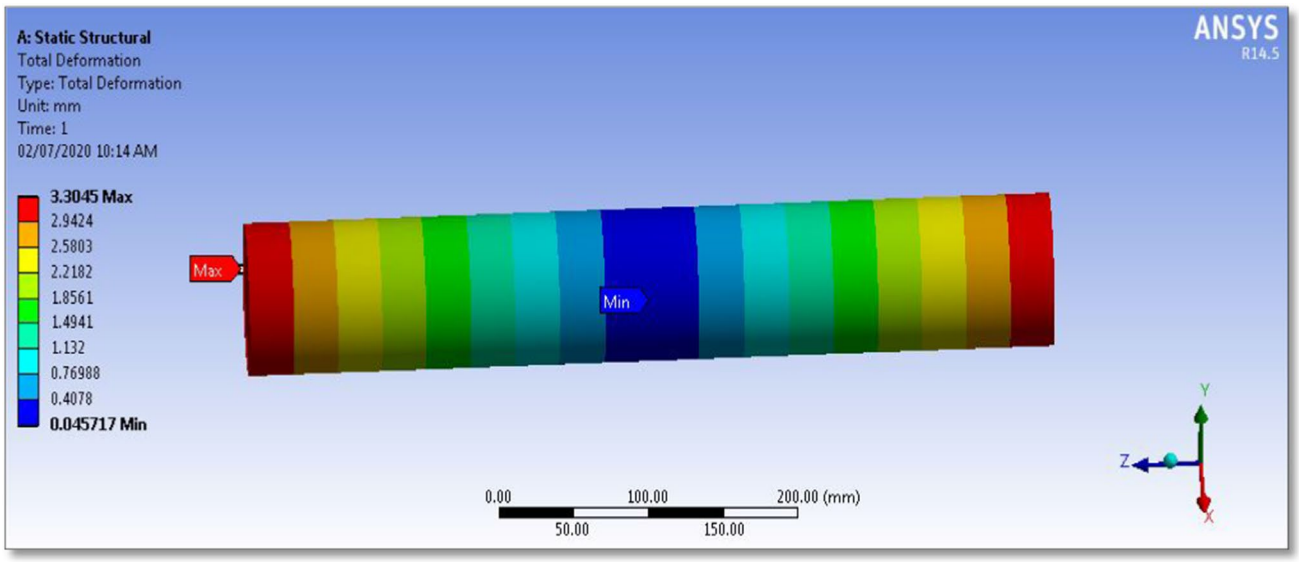

Fig. 15 Deflection under compressive force of 4.8 mm thick tube natural sand CFT specimen

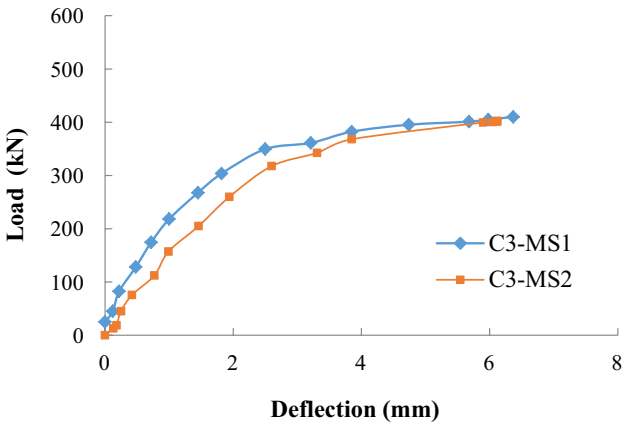

Fig. 16 Load- deflection curve for 3.2 mm thick tube artificial sand CFT specimens

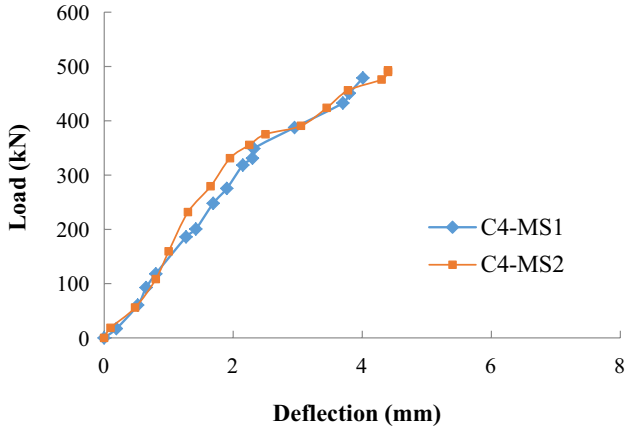

Fig. 17 Load- deflection curve for 4.0 mm thick tube artificial sand CFT specimens

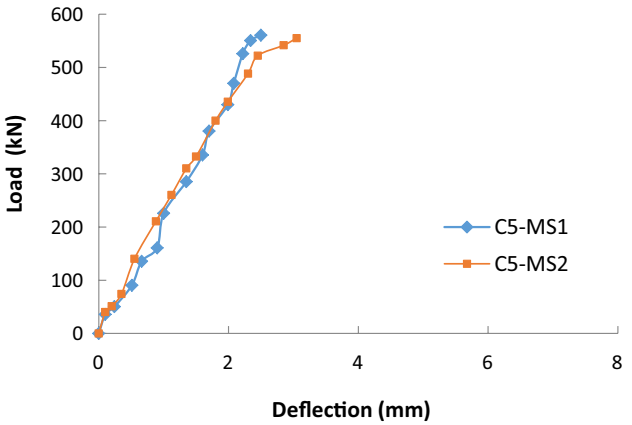

Fig. 18 Load- deflection curve for 4.8 mm thick tube artificial sand CFT specimens

Also, it is concluded that artificial sand CFT columns indicated the excellent ductile deformation behaviour during the axial compressive loading. As the thickness of tube increases, axial load-carrying capacity increases and lateral deformation decreases for both natural and artificial sand CFT columns. Also, the failure modes of specimens were observed outward buckling above the mid-height of CFT columns. The experimental and analytical results like load and deflection behaviour generally agreed with one another.

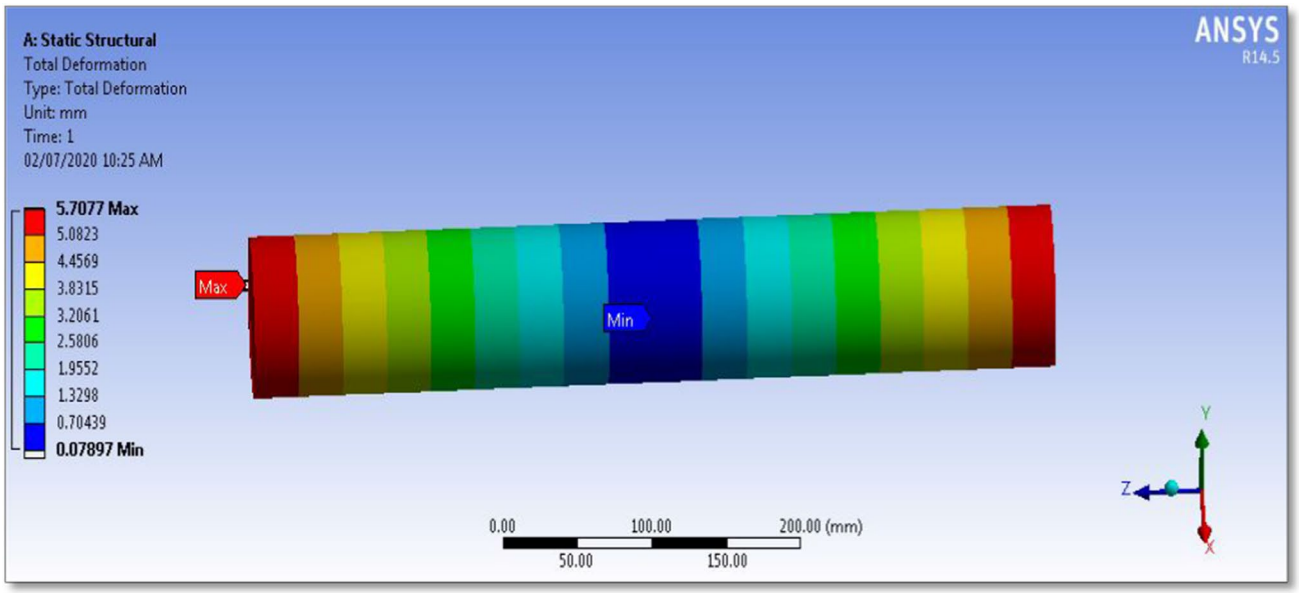

Fig. 19 Deflection under compressive force of 3.2 mm thick tube artificial sand CFT specimen

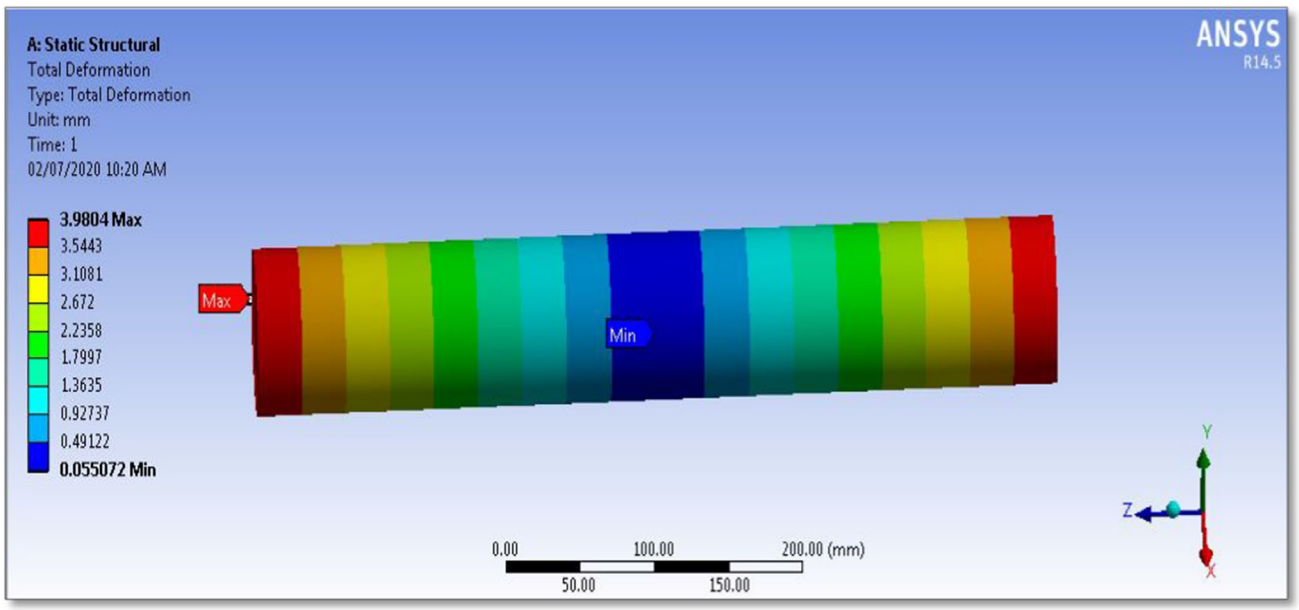

Fig. 20 Deflection under compressive force of 4.0 mm thick tube artificial sand CFT specimen

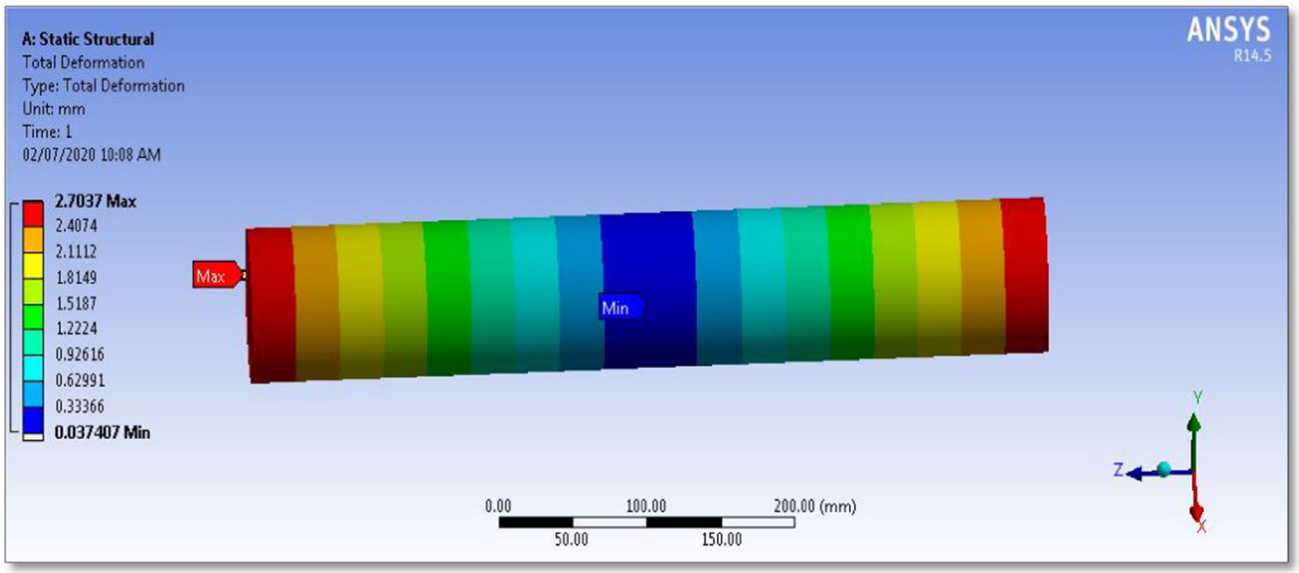

Fig. 21 Deflection under compressive force of 4.8 mm thick tube artificial sand CFT specimen

Table 5 Comparison of CFT specimen's load-carrying capacity

Specimen label	Experimental Load- carrying capacity Nue (kN)	Load-carrying capacity by EC-4 N_{EC4} (kN)	Nue/N_{EC4} (kN)	Load-carrying capacity by AISC 360-10 N_{AISC}(kN)	Nue/N_{AISC} (kN)
C3-RS1	400.02	316.36	1.26	284.18	1.41
C3-RS2	395.65	316.36	1.25	284.18	1.39
C4-RS1	472.25	380.35	1.24	345.59	1.37
C4-RS2	485.22	380.35	1.28	345.59	1.40
C5-RS1	535.01	431.06	1.24	398.50	1.34
C5-RS2	540.02	431.06	1.25	398.50	1.36
C3-MS1	423.88	322.02	1.32	295.20	1.44
C3-MS2	410.02	322.02	1.27	295.20	1.39
C4-MS1	489.98	385.72	1.27	350.02	1.40
C4-MS2	493.00	385.72	1.28	350.02	1.41
C5-MS1	555.20	436.30	1.27	405.90	1.37
C5-MS2	560.69	436.30	1.29	405.90	1.38

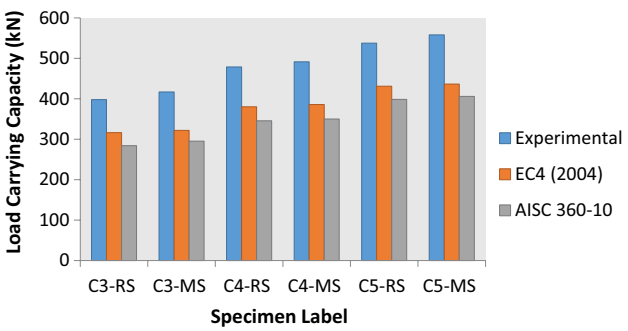

Fig. 22 Comparison of CFT specimen's load-carrying capacity

Compliance with ethical standards

Conflict of interest The author declare that they have no conflict of interest.

References

1. Han LH, Li W, Bjorhovde R (2014) Developments and advanced applications of concrete-filled steel tubular (CFST) structures: Members. J Constr Steel Res 100:211–228. https://doi.org/10.1016/j.jcsr.2014.04.016
2. Serras DN, Skalomenos KA, Hatzigeorgiou GD, Beskos DE (2016) Modeling of circular concrete-filled steel tubes

subjected to cyclic lateral loading. Structures 8:75–93. https://doi.org/10.1016/j.istruc.2016.08.008
3. de Oliveira WLA, De Nardin S, de CresceElDebs ALE, ElDebs MK (2009) Influence of concrete strength and length/diameter on the axial capacity of CFT columns. J Constr Steel Res 65:2103–2110. https://doi.org/10.1016/j.jcsr.2009.07.004
4. Ekmekyapar T, AL-Eliwi BJM (2016) Experimental behaviour of circular concrete filled steel tube columns and design specifications. Thin-Walled Struct 105:220–230. https://doi.org/10.1016/j.tws.2016.04.004
5. Zhou F, Young B (2009) Concrete-filled aluminum circular hollow section column tests. Thin-Walled Struct 47:1272–1280
6. Zhao XL, Pack JA (2009) Tests and design of concrete-filled elliptical hollow section stub columns. Thin-Walled Struct 47:617–628
7. Zhou F, Young B (2012) Numerical analysis and design of concrete-filled aluminium circular hollow section columns. Thin -Walled Struct 50:45–55
8. Choi I-R, Chung K, Kim C-S (2017) Experimental study on rectangular CFT columns with different steel grades and thicknesses. J Construct Steel Res 130:109–119
9. Zhu J-Y, Chan T-M (2019) Experimental investigation on steel-tube-confined-concrete stub column with different cross-section shapes under uniaxial-compression. J Constr Steel Res 162:105729
10. Sangeetha P, Senthil R (2017) Experimental behaviour of steel tubular columns for varying in filled concrete. Arch Civ Eng L18:149–160
11. Bo Wu, Yang Y (2013) Cyclic testing of circular steel tubular columns filled with demolished concrete blocks and fresh concrete. Thin-Walled Struct 66:50–61
12. Liao F-Y, Hou C et al (2019) Experimental investigation on sea sand concrete-filled stainless steel tubular stub columns. J Construct Steel Res 155:46–61
13. Xie J, Li J, Zhongyu Lu, Li Z, Fang C, Huang L, Li L (2019) Combination effects of rubber and silica fume on the fracture behaviour of steel-fibre recycled aggregate concrete. Constr Build Mater 203:164–173
14. Donza H, Cabrera O, Irassar EF (2002) High-strength concrete with different fine aggregate. Cem Concr Res 32:1755–1761
15. Khartode RR, Kulkarni DB (2016) Mix proportioning of HSC using manufactured sand. Int J Sci Res 2319–7064:1280–1283
16. Yang Y-F, Ma G-L (2013) Experimental behaviour of recycled aggregate concrete filled stainless steel tube stub columns and beams. Thin-Walled Struct 66:62–75
17. He An, Cai J, Chen Q-J, Liu X, Huang P, Tang X-L (2018) Seismic behaviour of steel-jacket retrofitted reinforced concrete columns with recycled aggregate concrete. Constr Build Mater 158:624–639
18. He An, Cai J, Chen Q-J, Liu X, Xue H, Chenjie Yu (2017) Axial compressive behaviour of steel-jacket retrofitted RC columns with recycled aggregate concrete. Constr Build Mater 141:501–516
19. Abhilash M, Sanyam Jhanjhari P, Parthiban JK (2019) Axial behaviour of semi-lightweight aggregate concrete-filled steel tube columns - A DOE approach. J Constr Steel Res 162:105614
20. Liu Z, Yiyan Lu, Li S, Liao J (2019) Axial behavior of slender steel tube filled with steel-fiber-reinforced recycled aggregate concrete. J Constr Steel Res 162:105748
21. Liu D (2004) Behaviour of high strength rectangular concrete-filled steel hollow section columns under eccentric loading. Thin-Walled Struct 42:1631–1644
22. Schneider SP (1998) Axially loaded concrete-filled steel tubes. J Struct Eng 124:1125–1138. https://doi.org/10.1061/(ASCE)0733-9445(1998)124:10(1125)
23. Han LH (2002) Tests on stub columns of concrete-filled RHS sections. J Construct Steel Res 58:353–372. https://doi.org/10.1016/S0143-974X(01)00059-1
24. Richard Liew JY, Xiong DX (2009) Effect of preload on the axial capacity of concrete-filled composite columns. J Constr Steel Res 65:709–722. https://doi.org/10.1016/j.jcsr.2008.03.023
25. Tan Q, Gardner L, Han L (2019) Performance of steel-reinforced concrete-filled stainless steel tubular columns at elevated temperature. Int J Struct Stab Dyn 19:1940002–1–1940018. https://doi.org/10.1142/S0219455419400029
26. Morkhade SG, Gupta LM (2019a) Behaviour of castellated steel beams: state of the art review. Electron J Struct Eng 19(1):39–48
27. Morkhade SG, Lokhande RS, Gund UD, Divate AB, Deosarkar SS, Chavan MU (2020) Structural behaviour of castellated steel beams with reinforced web openings. Asian J Civ Eng 21(6):1067–1078
28. Morkhade SG, Gupta LM (2015) Experimental study and rotational capacity of steel beams with web openings. Int J Civ Struct Eng 6(1):58–69
29. Morkhade SG, Gupta LM (2019b) Ultimate load behaviour of steel beams with web openings. Aust J Struct Eng 20(2):124–133
30. Morkhade SG, Shaikh S, Kumbhar A, Shaikh A, Tiwari R (2018) Comparative study of ultimate load for castellated and plain webbed beam. Int J Civ Eng Technol 9(8):1466–1476
31. Raut KV, Morkhade SG, Khartode RR, Ahiwale DD (2020) Experimental study on flexural behaviour of light steel hollow flange beam with various stiffening arrangements. Innov Infrastruct Solut 5:90. https://doi.org/10.1007/s41062-020-00345-4
32. AISC 360-10 (2010) Specification for structural steel buildings. American Institute of Steel Construction, Chicago, USA
33. EN 1994-1-1 (2004) Design of Composite steel and concrete structures. Eurocode 4, Brussels, Belgium
34. IS 11384-1985 (Reaffirmed 2003) Indian standard code of practice for composite construction in structural steel and concrete
35. IS 1239 Part-1 (2004) Indian standard steel tubes, tubular and other wrought steel fittings-specification. Bureau of Indian Standards, New Delhi
36. ASTM (2016) Standard test methods for tension testing of metallic materials. ASTM International, West Conshohocken, PA, USA. https://doi.org/10.1520/E0008_E0008M-16A
37. IS 10262 (2019) Concrete mix proportioning- guidelines. Bureau of Indian Standards, New Delhi
38. ANSYS Inc., Yuvi K (2012) Release 14.5 documentation. ANSYS, Canonsburg